Molecular Microbiology (2016) 101(2), 265–280 ■
doi:10.1111/mmi.13388
First published online 3 May 2016

A novel membrane anchor for FtsZ is linked to cell wall hydrolysis in *Caulobacter crescentus*

Elizabeth L. Meier,[1] Shiva Razavi,[2] Takanari Inoue[2,3] and Erin D. Goley[1]*
[1]*Department of Biological Chemistry, Johns Hopkins University School of Medicine, 725 N. Wolfe Street, Baltimore, Maryland, 21205, USA.*
[2]*Department of Biomedical Engineering, Johns Hopkins University School of Medicine, 720 Rutland Avenue, Baltimore, Maryland, 21205, USA.*
[3]*Department of Cell Biology, Johns Hopkins University School of Medicine, 855 N. Wolfe Street, Baltimore, Maryland, 21205, USA.*

Summary

In most bacteria, the tubulin-like GTPase FtsZ forms an annulus at midcell (the Z-ring) which recruits the division machinery and regulates cell wall remodeling. Although both activities require membrane attachment of FtsZ, few membrane anchors have been characterized. FtsA is considered to be the primary membrane tether for FtsZ in bacteria, however in *Caulobacter crescentus*, FtsA arrives at midcell after stable Z-ring assembly and early FtsZ-directed cell wall synthesis. We hypothesized that additional proteins tether FtsZ to the membrane and demonstrate that in *C. crescentus*, FzlC is one such membrane anchor. FzlC associates with membranes directly *in vivo* and *in vitro* and recruits FtsZ to membranes *in vitro*. As for most known membrane anchors, the C-terminal peptide of FtsZ is required for its recruitment to membranes by FzlC *in vitro* and midcell recruitment of FzlC in cells. *In vivo*, overproduction of FzlC causes cytokinesis defects whereas deletion of *fzlC* causes synthetic defects with *dipM*, *ftsE* and *amiC* mutants, implicating FzlC in cell wall hydrolysis. Our characterization of FzlC as a novel membrane anchor for FtsZ expands our understanding of FtsZ regulators and establishes a role for membrane-anchored FtsZ in the regulation of cell wall hydrolysis.

Accepted 29 March, 2016. *For correspondence. E-mail egoley1@jhmi.edu; Tel. (+1) 410-502-4931; Fax (+1) 410-955-5759.

Introduction

Bacterial cytokinesis is a multi-step process that couples dramatic reorganization of the cell envelope with faithful nucleoid replication and segregation. The tubulin-like GTPase FtsZ plays an essential role in bacterial cell division as a scaffold for the assembly of the division machinery (divisome) and, possibly, as a source of constrictive force (Osawa *et al.*, 2008; Osawa and Erickson, 2013). FtsZ forms a ring-like structure (the Z-ring) under the membrane at midcell and is thought to constrict to initiate cell division (Erickson *et al.*, 2010; Meier and Goley, 2014). All downstream components of the divisome require FtsZ for enrichment at midcell, including cell wall remodeling enzymes. A subset of divisome proteins interacts directly with and regulates FtsZ assembly, activity and structure.

One poorly understood class of FtsZ regulators mediates its membrane association. Most of what is known about FtsZ's membrane association comes from work in *Escherichia coli*. In that organism, inactivation of both of the known membrane anchors, FtsA and ZipA, destabilizes preformed Z-rings and blocks *de novo* Z-ring assembly (Pichoff and Lutkenhaus, 2002). This inspired a model wherein FtsZ must be tethered to the membrane to form a stable Z-ring. Moreover, transmission of constrictive force and communication with the cell wall remodeling machinery intuitively requires membrane attachment of the Z-ring. In *E. coli* cells, FtsA and ZipA perform unique roles beyond promoting Z-ring formation: FtsA recruits downstream division proteins and ZipA mediates pre-septal peptidoglycan synthesis (Pichoff *et al.*, 2012, 2015; Potluri *et al.*, 2012). These functional differences are borne out *in vitro* where each membrane anchor confers distinct dynamic properties to the membrane-associated FtsZ assemblies they mediate (Loose and Mitchison, 2014). However, the mechanisms by which these membrane-anchoring proteins differentially direct the function of FtsZ are poorly understood.

FtsA is considered the primary membrane tether for FtsZ in bacteria as it is broadly distributed and a gain-of-function mutation in FtsA renders ZipA non-essential in *E. coli* (Hale and de Boer, 1997; Geissler *et al.*, 2003). However, FtsA is not essential in *Bacillus subtilis*, where SepF and potentially

EzrA, also function as membrane anchors (Beall and Lutkenhaus, 1992; Jensen *et al.*, 2005; Singh *et al.*, 2007; Duman *et al.*, 2013). FtsA is entirely absent in some bacteria, including *Mycobacterium tuberculosis*, where SepF and FtsW are postulated to play membrane-tethering roles (Datta *et al.*, 2002; Gupta *et al.*, 2015). The diversity of membrane anchors across bacteria suggests unique, though poorly understood, roles in regulating FtsZ dynamics and activity during division.

FtsA is essential in the Gram-negative α-proteobacterium *Caulobacter crescentus*, known for its obligate asymmetric division and ease of synchronization (Osley and Newton, 1977; Ohta *et al.*, 1997; Christen *et al.*, 2011). However, FtsA arrives at the division site after stable Z-ring assembly and early, FtsZ-directed cell wall synthesis (Möll and Thanbichler, 2009; Goley *et al.*, 2011). If membrane tethering is, indeed, required for Z-ring formation, the late arrival of FtsA in *C. crescentus* implies the existence of additional membrane anchors that tether FtsZ to the membrane early in the cell cycle. *In vivo* and *in vitro* characterization of the FtsZ-binding protein FzlC suggests that it is one such candidate membrane tether. FzlC, a hypothetical protein with limited sequence similarity to heparinase II/III family proteins, is predicted to be cytoplasmic and is widely conserved in α-proteobacteria (Goley *et al.*, 2010b). FzlC binds directly to FtsZ polymers *in vitro* and requires FtsZ for its early recruitment to midcell *in vivo* (Goley *et al.*, 2010b). Interestingly, despite lacking a predicted membrane-binding domain, in cells depleted of FtsZ, FzlC has a patchy localization pattern that is reminiscent of membrane-associated proteins (Fig. 1A; Goley *et al.*, 2010b).

Based on its early recruitment to midcell, direct binding to FtsZ polymers and potential membrane localization, we hypothesized that FzlC could be an early membrane anchor for FtsZ before the arrival of FtsA. We pursued this hypothesis biochemically and found that FzlC indeed binds to membranes *in vivo* and *in vitro* and recruits FtsZ to membranes *in vitro*. *fzlC* overexpression led to impaired division while *fzlC* deletion caused synthetic cytokinesis defects in genetic backgrounds lacking other non-essential division genes implicated in cell wall hydrolysis. We postulate that FzlC is a redundant membrane anchor for FtsZ early in the cell cycle and improves the efficiency of cytokinesis through the regulation of cell wall hydrolysis.

Results

FzlC associates with membranes in vivo *and* in vitro

The localization of an mCherry-FzlC fluorescent fusion in *C. crescentus* cells depleted for FtsZ provided us with our first hint as to the role of FzlC during division (Fig. 1A; Goley *et al.*, 2010b). Under these conditions, FzlC appeared to associate with the cell membrane similar to the transmembrane fluorescent fusion, mCherry-FtsW (Fig. 1A). To support this observation, we took advantage of *E. coli* as a heterologous expression system for investigating FzlC association with membranes in cells. CFP-FzlC localized primarily to the periphery in *E. coli* cells, indicating that FzlC interacts with

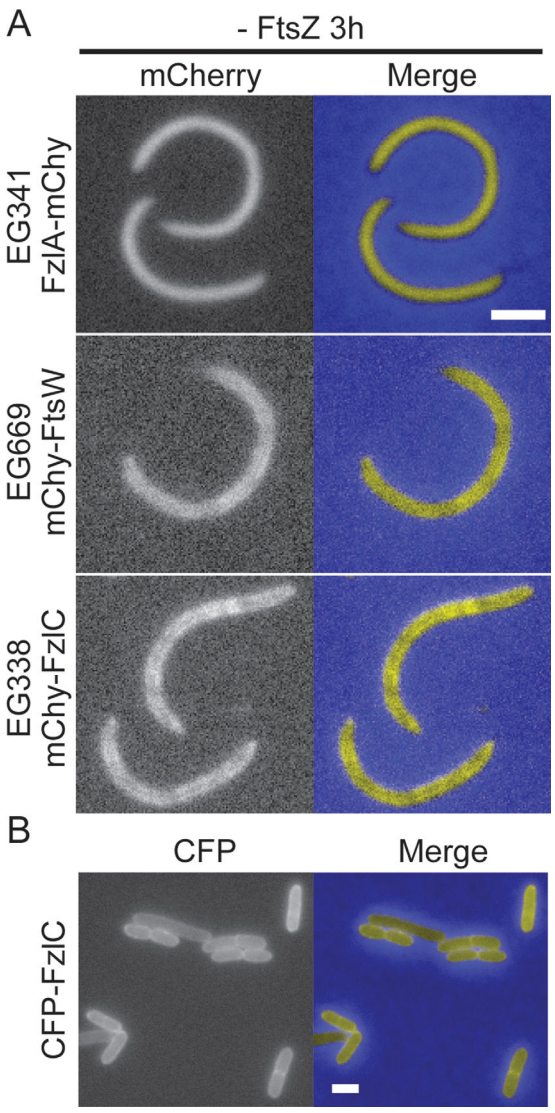

Fig. 1. FzlC localizes to membranes in *C. crescentus* and *E. coli* cells.
A. Fluorescence and merged micrographs of cells depleted of FtsZ for 3 h and expressing mCherry fusions to the indicated proteins induced with vanillate for 2 h. FzlA is diffuse in the cytoplasm (top row) while FtsW and FzlC display a patchy peripheral localization typical of membrane-associated proteins (middle and bottom rows).
B. Fluorescence and merged micrographs of cells producing CFP-FzlC after 2 h induction with 1% L-arabinose in *E. coli*. CFP-FzlC localizes to the periphery, indicating membrane association. Scale bars = 2 μm.

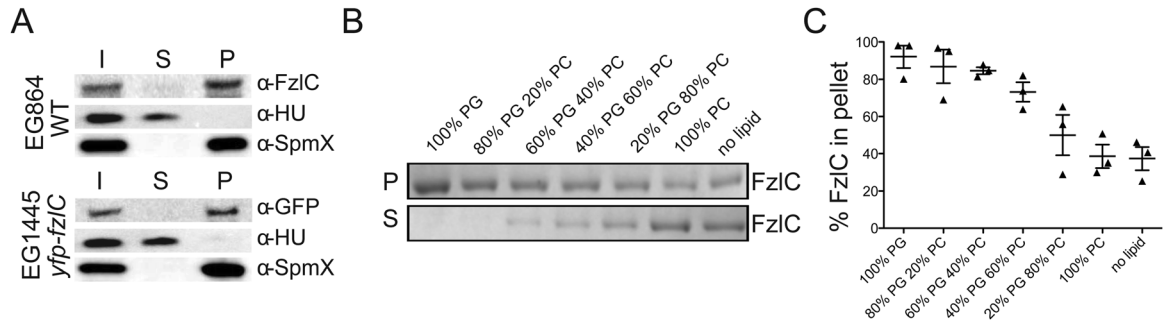

Fig. 2. FzlC binds to membranes *in vivo* and *in vitro*.
A. WT (EG864) or cells expressing *yfp-fzlC* as the only copy of *fzlC* (EG1445) were lysed and centrifuged to separate soluble (supernatant) and membrane (pellet) protein fractions. Whole cell lysate/input (I), soluble (S) and membrane (P) fractions were probed by immunoblotting for FzlC, as well as for SpmX (transmembrane protein) and HU (DNA-binding protein) as controls for membrane and soluble fractions respectively.
B. Coomassie stained gels of supernatant (S) and pellet (P) fractions after copelleting of FzlC with sucrose loaded unilamellar vesicles with the indicated molar percentages of phosphatidylglycerol (PG) and phosphatidylcholine (PC). Abundance of FzlC in the pellet indicates degree of binding to vesicles.
C. Quantification of FzlC lipid binding shown in (B). % FzlC in pellet was calculated by dividing the FzlC pellet band intensity by the total FzlC band intensity (pellet and supe) for each reaction. Error bars represent mean ± standard error of the mean (SEM) from three experimental replicates.

membranes in *E. coli* (Fig. 1B). In order to biochemically test if FzlC associates with membranes *in vivo*, we fractionated wild-type (WT) *C. crescentus* cells into membrane and soluble fractions and probed for FzlC by immunoblotting. Consistent with our fluorescence microscopy findings, FzlC was enriched in the pellet with the transmembrane protein control, SpmX, indicating association with membranes *in vivo* (Fig. 2A). We also fractionated *C. crescentus* cells expressing *yfp-fzlC* as the only copy of *fzlC*, since we used purified YFP-FzlC for most of the *in vitro* analyses described below. We found that YFP-FzlC was also enriched in the membrane fraction in this assay (Fig. 2A).

Since the primary sequence of FzlC lacks any predicted membrane binding motifs, we next asked if it could interact with membranes directly. The composition of *C. crescentus* membranes is ~90–95% phosphatidylglycerol (PG) and 5% cardiolipin (Contreras *et al.*, 1978). We therefore performed copelleting assays with purified FzlC and sucrose-loaded unilamellar vesicles containing a range of molar percentages of PG, which is anionic, and phosphatidylcholine (PC), which is net neutral and not found in *C. crescentus* membranes. FzlC copelleted with vesicles in a PG dose-dependent manner and did not bind to 100% PC vesicles (Fig. 2B and C). Thus, FzlC is a novel *C. crescentus* membrane-associated protein that binds the physiologically relevant lipid, PG, *in vitro*.

FzlC brings FtsZ to membranes

Since FzlC binds both to FtsZ filaments and membranes *in vitro*, we hypothesized that FzlC could function as a membrane anchor for FtsZ. The precedence of encapsulating bacterial proteins, including FtsZ membrane tethers, inside giant unilamellar vesicles (GUVs) inspired us to employ this minimal system for assaying FtsZ recruitment to membranes by FzlC (Cabre *et al.*, 2013; Osawa and Erickson, 2013). We used the inverted emulsion method to encapsulate YFP-FzlC and/or FtsZ-CFP +/– GTP inside GUVs with outer leaflets composed of 4:1 PC:phosphatidylserine (PS) and inner leaflets composed of 1:1 PG:PC (Pautot *et al.*, 2003; Luo *et al.*, 2014). YFP-FzlC alone localized robustly to the membrane while FtsZ-CFP alone remained lumenal under polymerizing (+GTP) and non-polymerizing (–GTP) conditions (Fig. 3A). When we combined YFP-FzlC and FtsZ-CFP +/– GTP, YFP-FzlC invariably localized to the membrane and it recruited FtsZ-CFP to the membrane in a GTP-dependent manner (Fig. 3B). Since FtsZ was recruited to the membrane only in the presence of FzlC and GTP, we conclude that FzlC can act as a membrane anchor for FtsZ polymers *in vitro*. We did not observe Z-ring assembly or FtsZ-dependent membrane deformation as reported for *E. coli* FtsZ-YFP-MTS or FtsZ and FtsA encapsulated inside liposomes (Osawa *et al.*, 2008; Osawa and Erickson, 2013). However, GUVs containing FzlC and FtsZ polymers were less stable than any of our other GUV preparations and we occasionally observed vesicle shrinkage under these conditions.

Since many FtsZ-binding proteins regulate the localization or activity of FtsZ by altering its superstructure or assembly dynamics, we assessed whether FzlC affected FtsZ polymer structure and/or GTPase activity. At equimolar concentrations of purified proteins, FzlC did not have any obvious effect on FtsZ filament

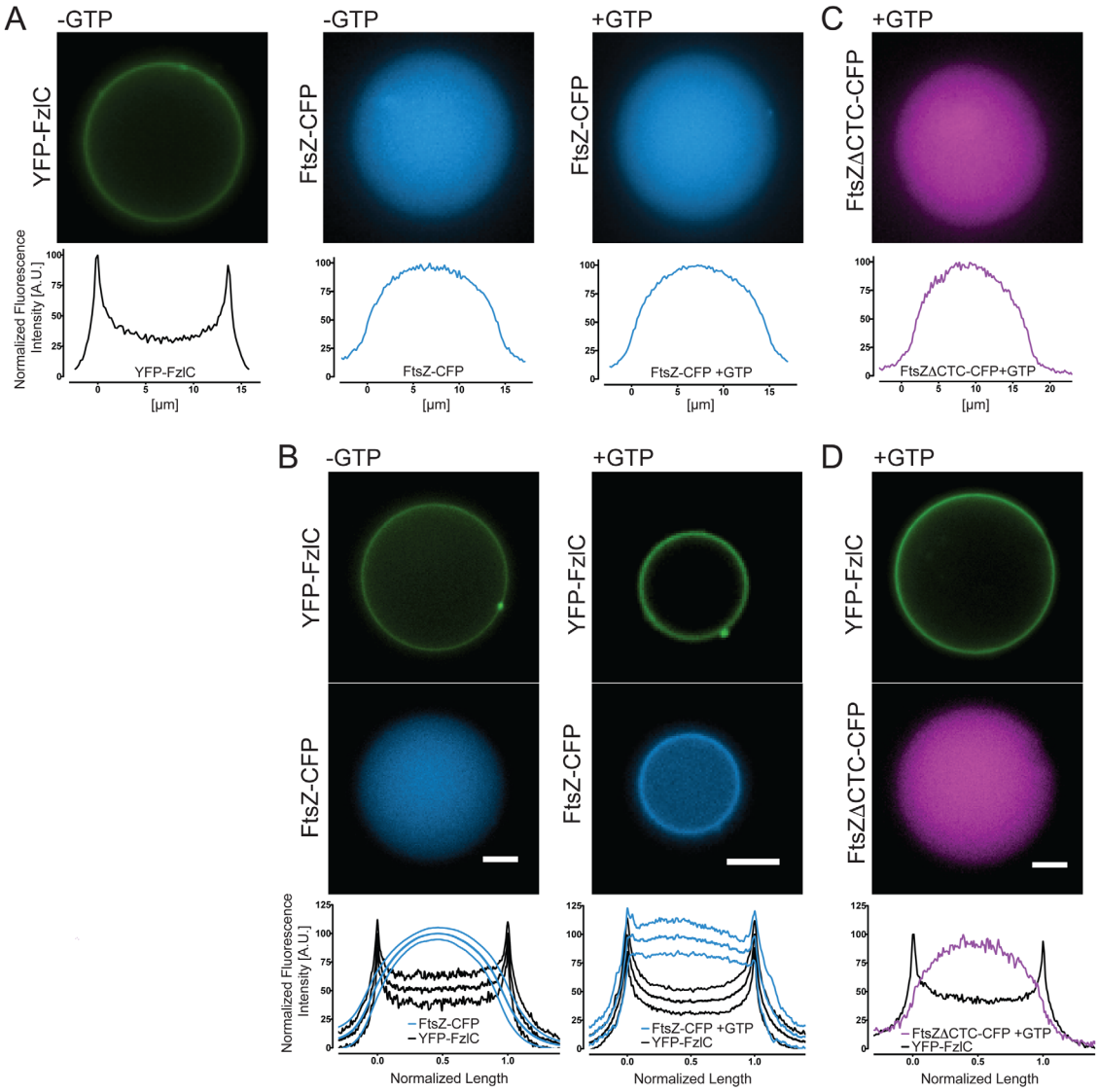

Fig. 3. YFP-FzlC recruits FtsZ-CFP polymers to membranes inside giant unilamellar vesicles (GUVs).
A–D. Fluorescence micrographs of representative GUVs containing the indicated proteins ± GTP. In (A, C and D), normalized fluorescence intensities from lines scans across the representative GUVs are shown, as localizations were uniform for each of these GUV populations. In (B), the mean normalized fluorescence intensities of line scans across 18 GUVs for each condition (± GTP) are presented and error bars (thin lines above and below middle line) represent standard deviation. Proteins were used at 2 μM, $MgCl_2$ was present at 2.5 mM in all FtsZ-containing reactions and, where indicated, GTP was used at 2 mM. Scale bars = 5 μm.

organization, as visualized using negative stain transmission electron microscopy (Supporting Information Fig. S1A). Although filament architecture was not appreciably affected, additional densities were observed along FtsZ filaments in the presence of FzlC, likely reflecting FzlC bound to filaments. The GTPase activity of FtsZ was also unaffected in the presence of FzlC, even when FzlC was added in molar excess (Supporting Information Fig. S1B). These data indicate that the primary biochemical activity of FzlC towards FtsZ is to serve as a membrane anchor.

FzlC and FtsZ interact in a CTC-dependent manner

The membrane anchoring proteins FtsA, ZipA and SepF all bind to the C-terminal conserved peptide (CTC) of FtsZ, which is highly conserved across bacteria (Vaughan *et al.*, 2004; Erickson *et al.*, 2010; Duman *et al.*, 2013). We sought to test if, like other canonical membrane tethers, FzlC interacts with FtsZ *via* the CTC using purified proteins *in vitro*. We first measured the polymerization activity of FtsZΔCTC-CFP and observed indistinguishable GTPase activity and only mildly reduced light scattering when compared to full length FtsZ-CFP (Supporting

Information Fig. S2A and B). To test if FzlC binds to the CTC, we encapsulated FtsZΔCTC-CFP +/– YFP-FzlC inside GUVs identical to those used for full length FtsZ as described above. Unlike full length FtsZ, under polymerizing conditions FtsZΔCTC-CFP remained completely luminal +/– YFP-FzlC (Fig. 3C and D). These data suggest that FzlC interacts with FtsZ by binding to the CTC.

To further validate the CTC dependence of FzlC-FtsZ association on membranes, we used an *in vitro* fluorescence resonance energy transfer (FRET) approach. When we combined purified YFP-FzlC and full-length FtsZ-CFP and excited at the CFP excitation wavelength, we observed minimal emission at the YFP wavelength, indicating a low basal level of FRET (Fig. 4). Addition of either GTP to induce FtsZ polymerization, or PG vesicles to induce membrane association did not change the FRET observed. However, we observed an increase in the FRET emission at 527 nm and corresponding decrease in the CFP emission at 475 nm leading to an increased FRET/CFP ratio – hallmarks of FRET indicating close proximity of FzlC and FtsZ – when YFP-FzlC and FtsZ-CFP were incubated in the presence of both GTP and PG vesicles (Fig. 4). This result suggested that we could use this FRET assay to ask if the CTC is required for the interaction of FtsZ polymers with FzlC on vesicles. When we combined YFP-FzlC with FtsZ lacking its CTC and fused to CFP (FtsZΔCTC-CFP), we saw complete abrogation of the GTP- and PG vesicle-induced FRET increase observed for full-length FtsZ-CFP (Fig. 4). Corroborating our GUV results, we conclude that recruitment of FtsZ polymers to membranes by FzlC *in vitro* requires the CTC.

To complement our *in vitro* analyses, we investigated whether FzlC requires the CTC to localize *in vivo* by imaging Venus-FzlC in a strain with vanillate-driven induction of the only copy of full-length *ftsZ* and xylose-driven induction of *ftsZΔCTC*. The localization of FtsA-Venus and ZapA-Venus were assessed in the same strain background as controls for proteins that do or do not require the CTC for localization respectively. After depleting full-length FtsZ and producing FtsZΔCTC for 6.5 h, ZapA-Venus localized to prominent, wide Z-rings. In contrast, FtsA-Venus and Venus-FzlC were both diffuse with only occasional, weak localization (Supporting Information Fig. S3). The loss of localization of FzlC upon depletion of full length FtsZ and production of FtsZΔCTC suggests that, like FtsA, it requires the CTC to associate with Z-rings *in vivo* (Din *et al*., 1998).

fzlC *overexpression causes a cell division defect*

Having validated FzlC as a novel membrane anchor for FtsZ in *C. crescentus*, we next sought to elucidate its

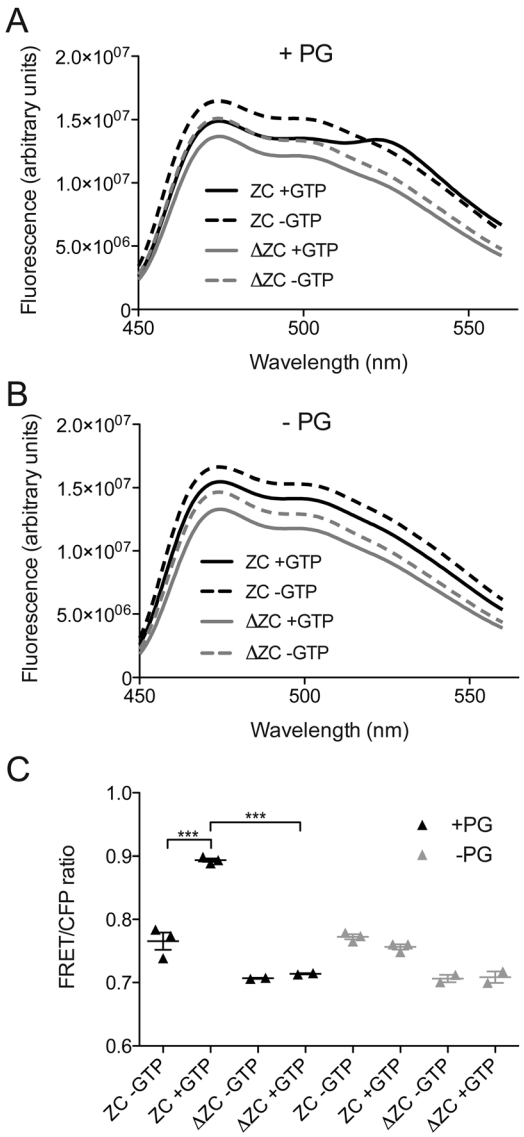

Fig. 4. FzlC and full length FtsZ, but not FtsZΔCTC, display FRET with GTP and PG vesicles *in vitro*.
A, B. Emission profiles of YFP-FzlC and FtsZ-CFP or FtsZΔCTC-CFP ± GTP in the presence (A) or absence (B) of PG vesicles after excitation at 435 nm.
C. FRET/CFP ratios of YFP-FzlC and FtsZ-CFP or FtsZΔCTC-CFP ± GTP in the presence or absence of PG vesicles. Error bars represent the mean FRET/CFP ratio ± SEM from three experimental replicates for reactions containing FtsZ-CFP and from two experimental replicates for reactions containing FtsZΔCTC-CFP; *** indicates $P < 0.001$ by one-way ANOVA. Labels: ZC = FtsZ-CFP/YFP-FzlC, ΔZC = FtsZΔCTC-CFP/YFP-FzlC

role during cell division. To this end, we constructed a strain containing a high copy plasmid for vanillate-inducible *fzlC* overexpression (EG891). We observed that, when compared to the empty vector control (EG890), cells overproducing FzlC were mildly elongated, with extended division sites, more pointed cell poles and longer doubling times (Fig. 5A and B; Supporting Information Table S1). We used principal

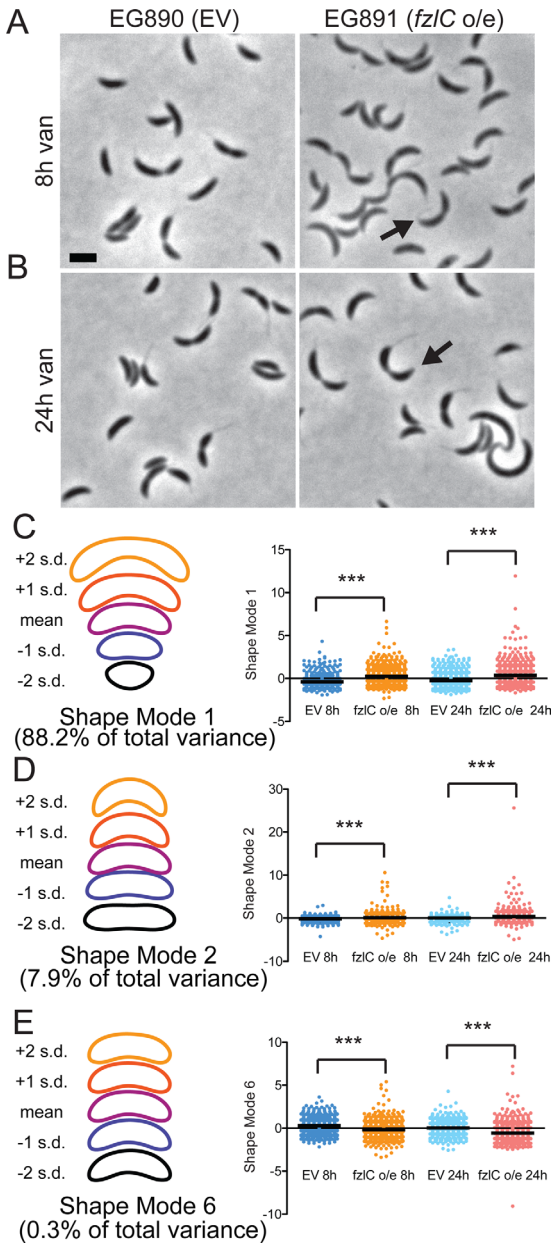

Fig. 5. High levels of FzlC interfere with efficient cytokinesis.
A,B. Phase contrast micrographs of cells containing empty vector (EG890) or vanillate-inducible *fzlC* overexpression vector (EG891) grown for 8 or 24 h in the presence of vanillate. The black arrows denote pointy poles (shape mode 6). Scale bar = 2 μm.
C–E. PCA of EG890 and EG891 produced seven different shape modes. Shown are scatter plots of shape modes 1, 2 and 6, which roughly correspond to length, curvature and pole shape respectively. Contours reflecting the mean shape and ±1 or 2 standard deviations (s.d.) from the mean in each shape mode are shown to the left of the corresponding scatter plot. The differences between EG890 (n = 582 and 752 cells at 8 and 24 h respectively) and EG891 (n = 658 and 817 cells at 8 and 24 h respectively) were statistically significant for these three shape modes; *** indicates $P < 0.001$ by Bonferroni's Multiple Comparison Test.

component analysis (PCA) to quantify modes of variation in cell shape after FzlC overproduction (Pincus and Theriot, 2007). Seven shape modes captured 99% of the variance in the data set of cells bearing the empty vector or vanillate-inducible *fzlC* grown with vanillate for 2, 6, 8 or 24 h. Shape modes 1 (roughly corresponding to cell length), 2 (cell curvature) and 6 (shape of the poles) were of particular interest as they most closely reflected the changes noted by manual inspection of cells upon *fzlC* overexpression. Indeed, at the 8 and 24 h time points, *fzlC* overexpressing cells (EG891) were significantly longer, more curved and had narrower cell poles compared to cells containing an empty vector (EG890), validating our qualitative observations of cell morphology (Fig. 5C–E). As cell poles are derived from cell division events, these FzlC-induced shape changes indicate aberrant cytokinesis in cells with excess FzlC.

Tagged variants of FzlC exhibit different phenotypes and localization ability

Interestingly, we found that when we replaced the native copy of *fzlC* with an N-terminal *mChy-fzlC* fusion (EG653), the phenotype was similar to *fzlC* overexpression. This cell division defect was specific to the N-terminal mCherry tag, as cells expressing C-terminal *fzlC-mChy* (EG859) or N-terminal *yfp-fzlC* (EG1445) fusions as the only copies of *fzlC* had morphologies and growth rates resembling WT (EG864) (Supporting Information Fig. S4A and C and Table S2). mChy-FzlC and YFP-FzlC localized to midcell with dynamics similar to FtsZ-YFP, while FzlC-mChy appeared more diffuse with only occasional midcell localization (Supporting Information Fig. S4A; Goley *et al.*, 2011). These data suggest that the C-terminus of FzlC is important for robust midcell localization.

Immunoblotting revealed FzlC to be present at very low levels in WT cells but to markedly increase after inducing *fzlC* expression with vanillate for 24 h (Supporting Information Fig. S4D). To ask whether differences in protein levels contributed to the phenotypes of the fluorescent FzlC fusions, we probed for FzlC by immunoblotting in cells with native *fzlC* replaced with *mChy-fzlC* (EG653), *fzlC-mChy* (EG859) or *yfp-fzlC* (EG1445). Cells with *mChy-fzlC* as the only copy of *fzlC* had strikingly higher levels of FzlC compared to cells with *fzlC-mChy* or *yfp-fzlC* (Supporting Information Fig. S4D), reinforcing our conclusion that excess FzlC impairs cytokinesis efficiency.

High levels of FzlC broaden the Z-ring in constricting cells

Since overexpressing *fzlC* produced a cytokinesis defect and FzlC tethers FtsZ polymers to membranes, we hypothesized that Z-ring structure may be affected in

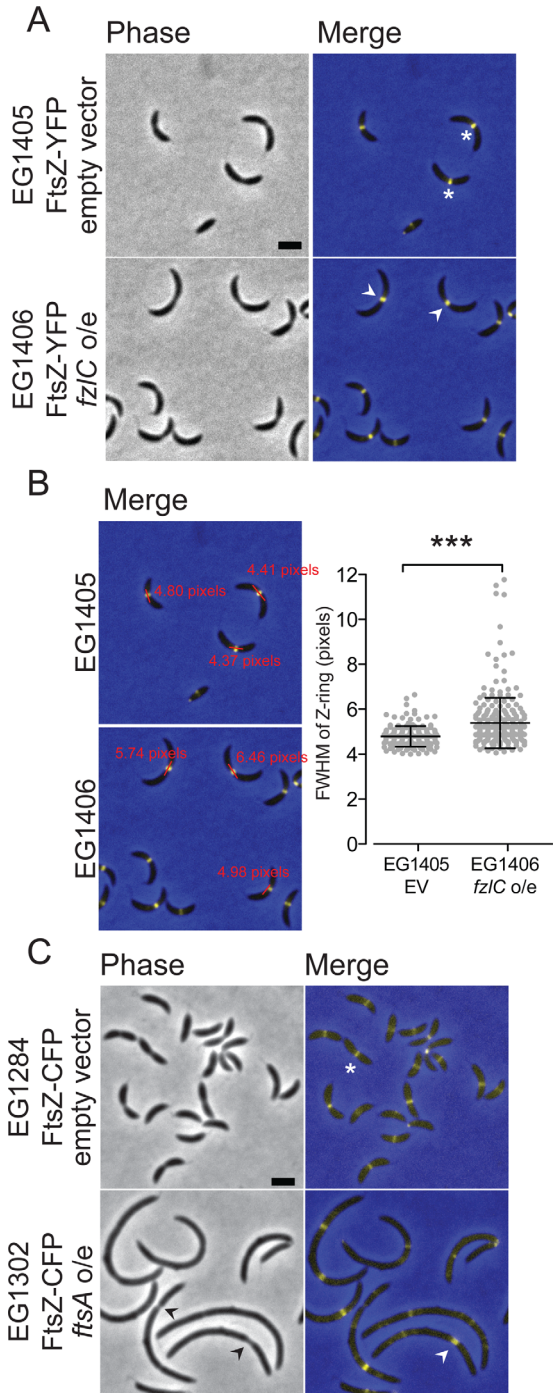

Fig. 6. High levels of FzlC broaden the Z-ring in constricting cells.
A. Phase contrast and merged fluorescent micrographs of cells containing xylose inducible *ftsZ-yfp* with an empty vector (EG1405) or vanillate-inducible *fzlC* overexpression vector (EG1406) grown in the presence of vanillate for 24 h and xylose for 1 h. The white asterisks denote focused Z-rings and white arrowheads denote more broad Z-rings at extended division sites.
B. Merged fluorescent micrographs from (A) with representative line scan full width half maximum (FWHM) measurements. Scatter plot shows the FWHM of Z-rings in cells with visible constrictions for EG1405 (n = 163) and EG1406 (n = 262); *** indicates $P < 0.001$ by unpaired t-test.
C. Phase contrast and merged micrographs of cells containing vanillate inducible *ftsZ-cfp* with empty vector (EG1285) or xylose-inducible *ftsA* overexpression vector (EG1302) grown in the presence of xylose for 4 h and vanillate for 1 h. The white asterisks denote focused Z-rings, the black arrowhead denotes deeply constricted sites and the white arrowheads denote a more diffuse Z-ring. Scale bars = 2 μm.

these cells. To address this hypothesis, we integrated a xylose-inducible copy of *ftsZ-yfp* at the *xylX* locus in cells containing a high copy plasmid for vanillate-inducible *fzlC* overexpression (EG1406) or an empty vector (EG1405). After growth with vanillate for 24 h, many *fzlC* overexpressing cells (EG1406) formed apparently normal Z-rings. In constricting cells, however, FtsZ was present in wider bands compared to the focused rings seen in cells containing an empty vector (EG1405) (Fig. 6A). To quantify this effect, we determined the full width at half maximum (FWHM) of FtsZ-YFP intensity along the long cell axis in cells with visible constrictions. Cells overexpressing *fzlC* had statistically higher FWHM values compared to the empty vector control, reflecting wider Z-rings in predivisional cells with excess FzlC (Fig. 6B).

FtsZ localization was even more obviously affected in cells expressing the *mChy-fzlC* fusion as the only copy of *fzlC* at its native locus (EG1404). Z-rings were wider and more dispersed, with patches of FtsZ occasionally observed on one side of the cell (Supporting Information Fig. S4B). We attribute this synthetic cell division defect to the combination of mild overexpression of *ftsZ-yfp* with high cellular levels of FzlC and/or the N-terminal mCherry tag affecting FzlC function (Supporting Information Fig. S4B and Table S2). We conclude that overproducing FzlC alters Z-ring organization in a manner consistent with the observed moderate reduction in cytokinesis efficiency.

As a point of comparison, we assessed Z-ring organization and cell morphology in cells overproducing the only other known membrane anchor in *C. crescentus*, FtsA. We integrated a vanillate-inducible copy of *ftsZ-cfp* at the *vanA* locus in cells containing an empty vector (EG1284) or a high copy plasmid for xylose inducible *ftsA* overexpression (EG1302). After inducing *ftsA* overexpression for 4 h, cells were filamentous and had multiple Z-rings with a range of widths, as well as patchy and diffuse FtsZ localization (Fig. 6C). The unique effects on cellular and Z-ring morphology upon overexpression of *fzlC* versus *ftsA* indicate distinct roles for these FtsZ membrane anchors *in vivo*.

FzlC *has synthetic interactions with other non-essential division genes*

To further define the role of FzlC in cell division, we next assessed the consequences of deleting *fzlC*. We found that *fzlC* was not essential: Δ*fzlC* (EG289) cells had WT

morphology, growth rate and Z-ring organization (Figs. 7A, 8A and Supporting Information S5A; Supporting Information Table S3; Goley *et al.*, 2010b). To test if *fzlC* had synthetic interactions with other non-essential division genes, we deleted *fzlC* in Δ*dipM* (EG1242), Δ*ftsE* (EG1162), Δ*zapA* (EG1232), Δ*tipN* (EG1299), Δ*kidO* (EG1298), Δ*ftsB* (EG1307), Δ*pbp1a* Δ*pbpY* Δ*pbpC* Δ*pbpZ* Δ*mtgA* ("Δ*5pbp*" a quintuple mutant lacking five of the six bifunctional PBPs encoded in *C. crescentus*) (Yakhnina and Gitai, 2013) (EG1509), or

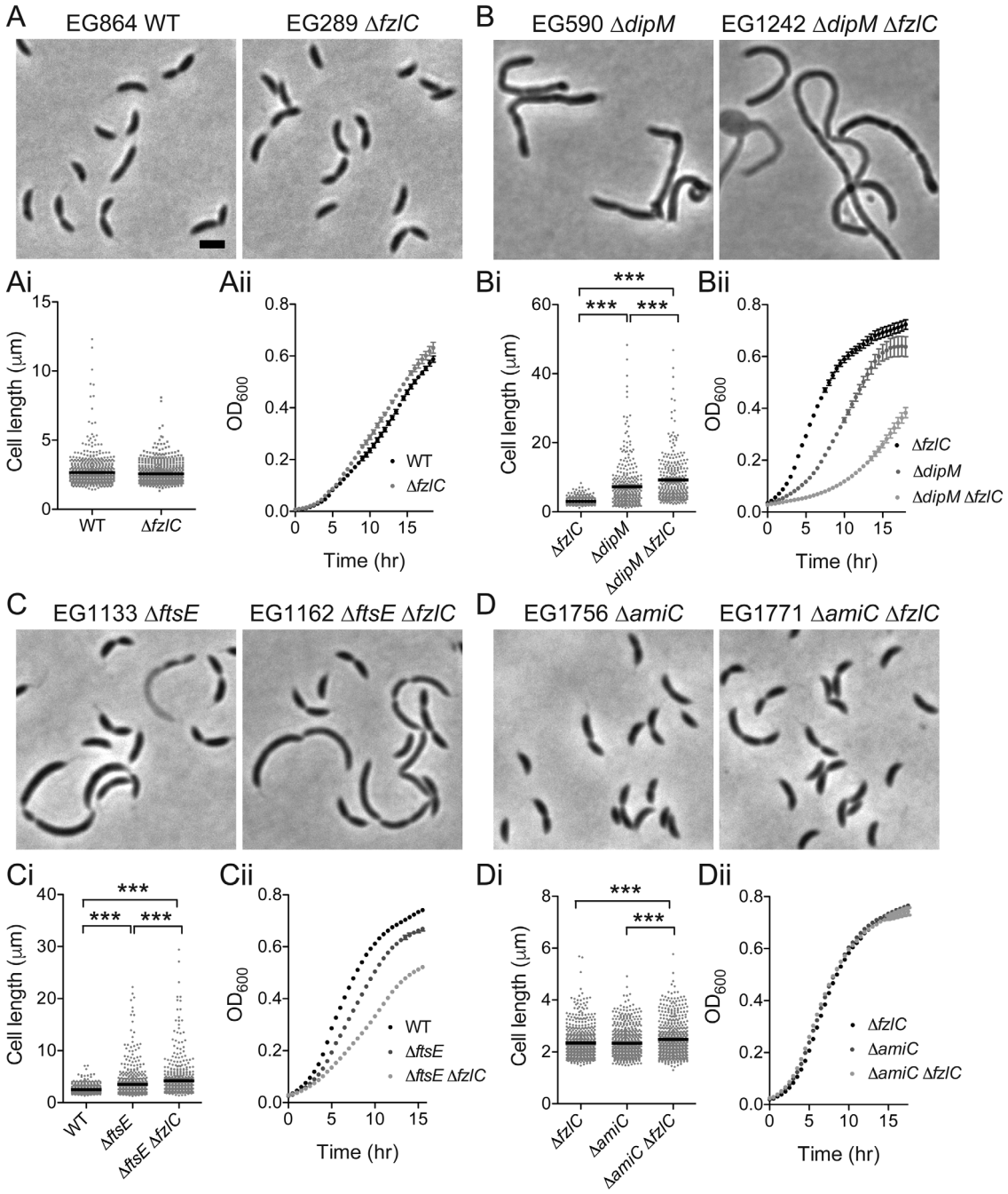

Fig. 7. Deletion of *fzlC* has synthetic interactions with non-essential division genes *dipM*, *ftsE* and *amiC*.
A–D. Phase contrast micrographs of cells with or without *fzlC* in WT, Δ*dipM*, Δ*ftsE*, or Δ*amiC* backgrounds.
Ai–Di. Cell length of strains in (A–D) (see Supporting Information Table S3 for sample sizes). Error bars represent the mean cell length ± SEM; *** indicates $P < 0.001$ by one-way ANOVA.
Aii–Dii. Growth curves of strains shown in (A–D). Scale bars = 2 μm.

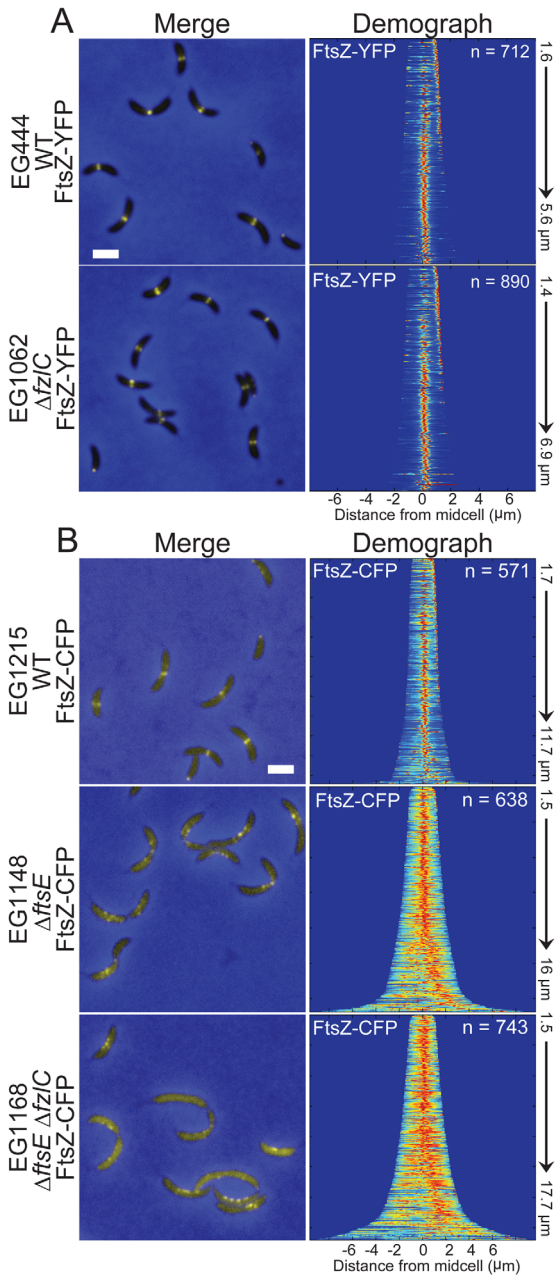

Fig. 8. Z-ring assembly is unaffected in Δ*fzlC* cells but aberrant in Δ*ftsE* cells.
A. Merged fluorescent (yellow) and phase contrast (blue) micrographs of cells with xylose-inducible *ftsZ-yfp* at the *xylX* locus in a WT (EG444) or Δ*fzlC* (EG1062) background. Demographs represent normalized signal profiles of FtsZ-YFP in cells arranged by increasing cell length.
B. Merged fluorescent (yellow) and phase contrast (blue) micrographs of cells with vanillate-inducible *ftsZ-cfp* at the vanillate locus in a WT (EG1215), Δ*ftsE* (EG1148), or Δ*ftsE* Δ*fzlC* (EG1168) background. Demographs represent signal profiles of FtsZ-CFP in cells arranged by increasing cell length. Scale bars = 2 μm.

Δ*amiC* (EG1771) strain backgrounds (Figs. 7B–D and Supporting Information S5A–F; Supporting Information Tables S3 and S4).

We looked for synthetic interactions wherein a mutant combination yielded statistically significant differences in growth rate and/or cell length between the double mutant and each of the corresponding single mutants. Of the genes tested, we found such interactions only with *dipM*, a peptidoglycan-binding putative endopeptidase; *ftsE*, the ATP-binding component of the ABC-transporter FtsEX complex; and the peptidoglycan amidase *amiC*. The synthetic double mutants (EG1242, EG1162 and EG1771) had significantly longer doubling times and/or cell lengths compared to either single mutant alone (Fig. 7, Supporting Information Table S3). Furthermore, all of the synthetic double mutants displayed, to different degrees, a chaining phenotype indicative of a late stage cell separation defect frequently associated with factors involved in cell wall hydrolysis (Fig. 7). In *E. coli*, *Streptococcus pneumoniae*, *B. subtilis* and *M. tuberculosis* FtsEX has been shown to activate peptidoglycan hydrolysis (Sham *et al.*, 2011; Yang *et al.*, 2011; Meisner *et al.*, 2013; Mavrici *et al.*, 2014). Thus, the synthetic division defects upon deletion of *fzlC* in cells lacking DipM, FtsE, or AmiC suggest that *fzlC* is specifically implicated in the regulation of cell wall hydrolysis. This synthetic relationship appears specific for cell wall hydrolysis, as opposed to synthesis, as no genetic interaction was observed with the quintuple glycosyltransferase mutant ("Δ*5pbp*"), nor was any effect observed on the location or timing of cell wall synthesis in cells lacking *fzlC* (Supporting Information Fig. S6). Moreover, deleting *fzlC* had no effect on the sensitivity of β-lactamase deficient *C. crescentus* to mecillinam and cephalexin, inhibitors of the transpeptidases, PBP2 and PBP3 respectively (Supporting Information Fig. S5G and H).

fzlC *overexpression partially rescues the cytokinesis defects of* ΔftsE

The synthetic interaction between *fzlC* and *ftsE* was of particular interest to us since, beyond regulating cell wall hydrolysis, FtsEX hypothetically could function as a membrane tether for FtsZ (Goley *et al.*, 2011). In *E. coli*, FtsE is proposed to bind FtsZ while FtsX is embedded in the inner membrane (Corbin *et al.*, 2007); this topology would allow for recruitment of FtsZ to membranes. Moreover, FtsE is among the first proteins recruited to the incipient division site (Goley *et al.*, 2011). Consistent with Δ*fzlC* cells' lack of morphological and growth defects, Z-ring assembly was similarly unaffected in Δ*fzlC* cells compared to WT (Fig. 8A). In contrast, we observed striking mislocalization of FtsZ in Δ*ftsE* cells: FtsZ was more diffuse and frequently formed clusters of puncta instead of focused Z-rings (Fig. 8B). The mislocalization of FtsZ was even more pronounced in Δ*ftsE*

Δ*fzlC* cells as demonstrated by the mostly diffuse FtsZ-CFP signal in cells and in the corresponding demograph (Fig. 8B). We hypothesized that the synthetic effect on FtsZ localization in Δ*ftsE* Δ*fzlC* cells was due to partially redundant functions of FtsE and FzlC as membrane tethers. To test this hypothesis, we overexpressed *fzlC* in Δ*ftsE* cells for 24 h and observed partial rescue of growth rate and cell length compared to the empty vector control (Fig. 9A–C; Supporting Information Table S5). Correspondingly, overproducing FzlC in Δ*ftsE* cells largely restored the focused, midcell localization of FtsZ (Fig. 9D). The ability of high levels of FzlC to partially rescue Z-ring localization and function in Δ*ftsE* cells suggests FzlC and FtsEX, in addition to regulating cell wall hydrolysis, may function as redundant membrane anchors for FtsZ during division.

Discussion

It is becoming increasingly apparent that the mode of membrane attachment of FtsZ defines a control point for the assembly and function of the Z-ring. Our discovery that FzlC binds and recruits FtsZ to membranes *in vivo* and *in vitro* fulfills the necessary requirements to define it as a new membrane anchor for FtsZ. FzlC recruits FtsZ polymers to membranes in a CTC-dependent manner, placing it in the company of FtsA, ZipA and SepF in ensuring that FtsZ is positioned with its flexible C-terminal linker separating the polymerizing GTPase domain from the membrane attachment point (Erickson *et al.*, 2010; Duman *et al.*, 2013). *In vivo*, high levels of FzlC cause defects in growth rate and morphology as well as a moderate alteration in Z-ring structure in constricting cells. Although non-essential, *fzlC* has synthetic interactions with a subset of other non-essential division genes, *dipM*, *ftsE* and *amiC*: these synthetic effects suggest that FzlC, like these other factors, acts in the regulation of peptidoglycan hydrolysis.

In light of the late arrival of FtsA to the division plane in *C. crescentus*, we originally set out to answer the question of how FtsZ is tethered to the membrane early in the cell cycle. Although we proposed FzlC as an attractive candidate for mediating membrane attachment of FtsZ before the arrival FtsA, Δ*fzlC* cells still assemble Z-rings with localized new cell wall synthesis early in the cell cycle (Figs. 8A and Supporting Information Fig. S6). Moreover, we did not observe a synthetic defect with Δ*fzlC* and loss of *zapA*, an FtsZ-binding protein important for assembly of focused Z-rings (Supporting Information Fig. S5B; Buss *et al.*, 2013), as would be predicted if FzlC were important for early Z-ring assembly. This implies either that FzlC acts redundantly with another membrane anchor or that membrane attachment of FtsZ is not strictly required for Z-ring assembly and activity. If the former is true, the most likely candidate is the highly conserved FtsEX ABC transporter complex (Goley *et al.*, 2011). The synthetic interaction between *fzlC* and *ftsE* (Figs. 7–9) further supports the possibility that FtsEX plays a redundant membrane-anchoring role with FzlC

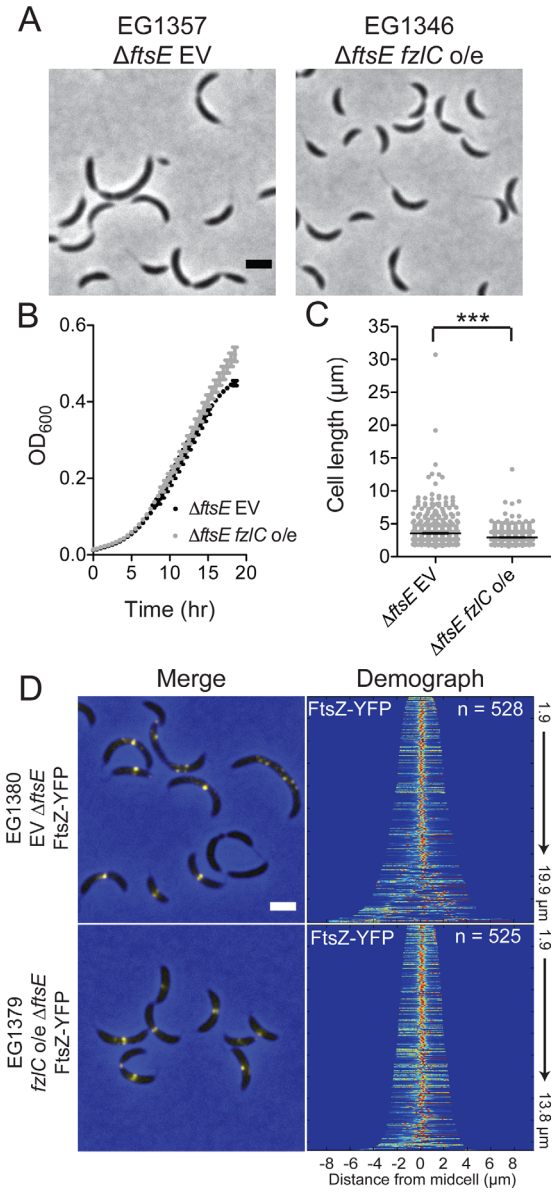

Fig. 9. High levels of FzlC partially rescue the morphological, growth and Z-ring structure defects in Δ*ftsE* cells.
A. Phase contrast micrographs of Δ*ftsE* cells with an empty vector (EG1357) or vanillate-inducible *fzlC* overexpression vector (EG1346) grown in the presence of vanillate for 24 h.
B,C. Growth curves and cell lengths of EG1357 and EG1346 cells shown in (A); *** indicates $P < 0.001$ by one-way ANOVA.
D. Xylose-inducible *ftsZ-yfp* at the *xylX* locus in an EG1357 or EG1346 background. Demographs represent normalized signal profiles of FtsZ-YFP in cells arranged by increasing cell length. Scale bars = 2 μm.

and FtsA in *C. crescentus*. Likewise, the ability of FzlC to positively regulate Z-ring assembly in the absence of FtsE underscores FzlC's role as a physiologically relevant membrane anchor. However, the putative activity of FtsEX as an early membrane anchor awaits biochemical and cytological confirmation.

Overproduction of FzlC led to broader Z-rings, especially at extended division sites, and morphological defects consistent with a slowed constriction rate (Figs. 5 and 6). This phenotype is markedly different from overproduction of FtsA, which causes filamentation and formation of Z-rings that are non-functional for constriction (Fig. 6C). These observations reinforce the idea that all membrane anchors are not functionally equivalent, even if they bind FtsZ and membranes in similar ways. Depletion of FtsA causes cells to grow into filaments with deep, broad constrictions similar in morphology to those in FzlC-overproducing cells (Martin *et al*., 2004). We postulate that excess FzlC, which is normally present at very low levels, competes with FtsA for binding to the CTC of FtsZ, titrating away FtsZ that is normally free to bind FtsA and complete constriction. Interestingly, replacing the native copy of *fzlC* with an N-terminal *mChy-fzlC* fusion increases FzlC levels and mimics the overexpression phenotype (Supporting Information Fig. S4). This mCherry tag could potentially mask an N-terminal degron sequence, which normally promotes high turnover of FzlC and contributes to the low WT protein levels. It is possible that FzlC is upregulated or stabilized to control cytokinesis under particular environmental conditions. However, a survey of common stresses including temperature, osmotic stress, oxidative stress and starvation has not revealed a condition under which FzlC is upregulated or essential.

The specific synthetic interactions between deletion of *fzlC* and loss of *dipM*, *ftsE* and *amiC* implicate FzlC in pathways impinging on cell wall hydrolysis. Cell wall hydrolase activity is particularly important in the late stages of cytokinesis, where hydrolases are required to split the peptidoglycan that holds the two daughter cells together (Lee and Huang, 2013). Though incompletely understood, coupling between Z-ring constriction and cell wall hydrolase activity was first proposed in *E. coli*. In that organism, local activation of the cell wall amidases, AmiA and AmiB, at the division site requires EnvC (Uehara *et al*., 2010), which is in turn activated by FtsX (Meisner *et al*., 2013). The activity of FtsX is proposed to be regulated by its partner, FtsE. Since FtsE is thought to directly interact with FtsZ, this series of interactions may transmit information about the state of the Z-ring to cell wall hydrolases in the periplasm, allowing for coordinated membrane and cell wall invagination (Yang *et al*., 2011).

Though the details of these interactions differ from organism to organism, activation of cell wall hydrolysis by FtsX appears to be a conserved mechanism for regulating envelope constriction (Sham *et al*., 2011; Meisner *et al*., 2013; Mavrici *et al*., 2014). In *C. crescentus*, splitting of septal peptidoglycan occurs synchronously with peptidoglycan synthesis and inner membrane constriction, rather than being delayed, as it is in *E. coli* and *B. subtilis* (Judd *et al*., 2005). However, relatively little is known about the molecular mechanisms regulating these processes. In particular, the identity of the hydrolase regulated by FtsX in *C. crescentus*, if it exists, is unknown: there are no clear homologs of AmiA, AmiB, or EnvC encoded in its genome. Complicating matters further, DipM is a LytM family protein similar to *E. coli* NlpD, which activates the amidase, AmiC, yet DipM does not activate AmiC in *C. crescentus* (Goley *et al*., 2010a; Möll *et al*., 2010). The phenotypes associated with loss of DipM, AmiC, or FtsE are dissimilar (Fig. 7), suggesting that these factors act in distinct, though perhaps partially redundant, pathways in this organism. While our genetic interaction analyses did not reveal which hydrolase(s) FzlC may ultimately activate, its synthetic interactions reinforce the concept of coordination between Z-ring activity and cell wall splitting and identify a novel route from FtsZ to the cell wall via FzlC membrane attachment.

It has long been hypothesized that in *E. coli* FtsZ must be attached to the membrane to assemble stable Z-rings (Pichoff *et al*., 2002). At least in *C. crescentus*, however, the CTC appears to be dispensable for Z-ring formation as Z-rings still form in cells expressing FtsZΔCTC and depleted of full-length FtsZ (Supporting Information Fig. S3; Sundararajan *et al*., 2015). As all known membrane-tethering proteins bind FtsZ through the CTC, these observations indicate that membrane attachment is not strictly necessary for Z-ring assembly. However, in *C. crescentus*, Z-rings containing FtsZΔCTC were non-functional and dominant negative, indicating loss of essential CTC binding partners and/or an important role for membrane attachment beyond stable Z-ring assembly (Supporting Information Fig. S3). The transduction of FtsZ-based constrictive force to the inner membrane and/or the coupling of Z-ring structure and dynamics with cell wall remodeling are likely candidates for downstream events requiring membrane-tethered FtsZ. Further supporting the connection between membrane-associated FtsZ and the cell wall, the SepF homolog recently identified in *M. tuberculosis* was reported to bind not only FtsZ and membranes, but also MurG, an essential enzyme in the synthesis of the lipid II peptidoglycan precursor (Gupta *et al*., 2015). Our data demonstrate that the function of FzlC similarly

transcends passive membrane anchoring, as it helps to translate "inside" Z-ring dynamics to "outside" cell wall remodeling events. These findings support a paradigm in which membrane anchors for FtsZ are key regulators in the coordinated constriction of the cell envelope during bacterial cytokinesis.

Experimental procedures

Bacterial strains and growth conditions

C. crescentus NA1000 strains were grown in peptone yeast extract (PYE) medium at 30°C (Sundararajan *et al*., 2015). Additives and antibiotics were used at the following concentrations in liquid (solid) media for *C. crescentus*: xylose 0.3 (0.3)%, glucose 0.2 (0.2)%, vanillate 0.5 (0.5) mM, gentamycin 1 (5) μg ml^{-1}, kanamycin 5 (25) μg ml^{-1}, spectinomycin 25 (100) μg ml^{-1}, streptomycin (5 μg ml^{-1}), cephalexin 1.25 and 2 μg ml^{-1} and mecillinam 12 and 18 μg ml^{-1}. Before changes in induction conditions, cells were washed two to three times in plain media. Growth rate analyses were performed in 96-well plates with shaking at 30°C using a Tecan Infinite 200 Pro plate reader. *E. coli* strain BL21-Gold(DE3) was grown in Luria-Bertani (LB) broth at 30°C. Antibiotics were used at the following concentrations for *E. coli*: ampicillin 50 μg ml^{-1} and tetracycline 12 μg ml^{-1}. Small-scale synchrony of *C. crescentus* cells was performed as in (Goley *et al*., 2011). Strains and plasmids used in this study are included as Supplementary Material.

Heterologous E. coli *expression system*

E. coli strain BL21-Gold(DE3) was transformed with a plasmid for arabinose inducible expression of *cfp-fzlC* (pEG908). To continuously maintain the cultures in log phase, a single colony was inoculated into fresh LB in the morning and grown at 30°C until the OD_{600} reached ~0.1. *cfp-fzlC* expression was then induced with 1% L-arabinose for 2 h at 30°C and imaged.

Light microscopy and image analysis

Cells were imaged during the log phase of growth after immobilization on 1% agarose pads. Light microscopy was performed on a Nikon Eclipse Ti inverted microscope equipped with a Nikon Plan Fluor × 100 (numeric aperture 1.30) oil Ph3 objective and Photometrics CoolSNAP HQ cooled CCD (charge-coupled device) camera. Chroma filter cubes were used as follows: ET-EYFP for YFP and ET-ECFP for CFP, ET-dsRED for mCherry and rhodamine and ET-DAPI for HADA. Images were processed in Adobe Photoshop. Automated cell length analysis was performed using MicrobeTracker (Sliusarenko *et al*., 2011). Algorithm 4 was used for determining cell outlines, with the following parameter change: areaMin=150. Principal component analysis was performed using CellTool (Pincus *et al*., 2007). Binary masks of phase contrast images were generated in ImageJ and manually curated in Adobe Photoshop to remove signal from incomplete cells at the edges of the field, from cells that were touching, or from debris. The shape model was built to capture 99% of the variation in the *fzlC*-overexpressing and empty vector populations. FWHM of Z-ring width in cells overexpressing *fzlC* was determined by manually drawing a line through Z-rings in constricted cells in ImageJ and using an ImageJ macro to fit a Gaussian to the intensity profile and calculate the FWHM of the Gaussian.

Antibodies and immunoblotting

Purified *C. crescentus* His_6-FzlC was used to immunize a rabbit for antibody production (Josman, LLC). To affinity purify the antibody, His_6SUMO-FzlC was coupled to Affigel 10 resin and incubated with serum. FzlC-specific antibodies were serially eluted with 0.2 M glycine pH 2.5 and 6 M guanidine, and dialyzed into Tris-buffered saline. The guanidine elution had higher specificity and was used for all future immunoblots. Specificity for FzlC was demonstrated by immunoblotting lysates from strains with *fzlC* deleted or overexpressed and observing elimination or amplification respectively, of the signal at the expected molecular weight of FzlC (predicted 61 kDa; for example, Figs. 2 and Supporting Information Fig. S4). For immunoblotting against whole-cell lysates, cells were harvested in the log phase of growth and lysed in SDS-PAGE loading buffer by boiling for 5 min. SDS-PAGE and transfer of protein to nitrocellulose membrane were performed using standard procedures. FtsZ antiserum was used at 1:20,000 dilution (Sundararajan *et al*., 2015). FzlC antibody was used at 1:2,000 or 1:5,000 dilutions. SpmX antiserum was used at 1:50,000 dilution (Radhakrishnan *et al*., 2008). HU antiserum was used at 1:5,000 dilution (Bowman *et al*., 2010).

Protein purification

FtsZ and FtsZ variants were overproduced and purified as described previously (Goley *et al*., 2010b) with slight modifications. Rosetta (DE3) pLysS *E. coli* cells bearing constructs for expression of FtsZ (pEG012), His_6-FtsZ-CFP (pEG448), or His_6-FtsZΔCTC-CFP (pEG1170) were grown in LB at 37°C to OD_{600} of 0.8–1.0 before induction with 0.5 mM isopropylthiogalactoside (IPTG) for 3–4 h. Cells were harvested by centrifugation at 6,000*g* for 10 min at 4°C, resuspended in 30 ml Buffer QA (50 mM Tris-HCl, pH 8.0, 50 mM KCl, 1 mM EDTA, 1 mM β-mercaptoethanol and 10% glycerol) per 0.5 to 1 liter of culture, snap-frozen in liquid nitrogen and stored at −80°C until purification. Cell suspensions were thawed at 37°C, one Mini Complete Protease Inhibitor tablet (Roche) was added per 30 ml, lysozyme was added to 1 μg ml^{-1}, phenylmethyl sulphonyl fluoride (PMSF) was added to 2 mM and DNase I (New England Biolabs) was added to 2 units ml^{-1} final concentrations. Cell suspensions were incubated for 30–60 min at room temperature or 4°C, sonicated, and centrifuged at 15,000*g* for 30 min at 4°C. Supernatant was filtered and loaded on two HiTrap Q HP 5 ml columns (GE Life Sciences) joined in tandem and equilibrated in Buffer QA. Protein was eluted using a linear KCl gradient from 50 to 500 mM over 20 column volumes. Peak fractions containing FtsZ were combined and ammonium sulfate was

added to 20% saturation. Ammonium sulfate precipitate was recovered with centrifugation at 10,000*g* for 10 min at 4°C. Precipitates were either stored on ice overnight or immediately resuspended in FtsZ Storage Buffer (50 mM HEPES-KOH pH 7.2, 50 mM KCl, 0.1 mM EDTA, 1 mM β-mercaptoethanol and 10% glycerol) and consequently applied to a Superdex 200 10/300 GL (GE Life Sciences) equilibrated in FtsZ Storage Buffer. Peak fractions were combined, concentrated if necessary, snap-frozen in liquid nitrogen and stored at −80°C.

To purify His_6-SUMO-FzlC, Rosetta (DE3) pLysS *E. coli* cells bearing plasmid pEG605 were grown at 30°C to OD_{600} of 0.8–1.0 before induction with 30 μM IPTG overnight at 15°C (Guo *et al.*, 2007). Cells were harvested by centrifugation at 6,000*g* for 10 min at 4°C, resuspended in 30 ml FzlC Column Buffer A (50 mM Tris-HCl pH 8.0, 1 M KCl, 20 mM imidazole, 1 mM β-mercaptoethanol and 20% glycerol) per 0.5 to 1 liter of culture, snap-frozen in liquid nitrogen and stored at −80°C until purification. Cell suspensions were thawed at 37°C and lysozyme was added to 1 μg ml^{-1}, $MgCl_2$ was added to 2.5 mM and DNase I (New England Biolabs) was added to 2 units ml^{-1} final concentrations. Cell suspensions were incubated for 30–60 min on ice, sonicated and centrifuged at 15,000*g* for 30 min at 4°C. Supernatant was filtered and supplemented with 3 mM ATP before loading on a HisTrap FF 1 ml column (GE Life Sciences) equilibrated in FzlC Column Buffer A. Protein was eluted at 30% FzlC Column Buffer B (same as Column Buffer A except 1 M imidazole). Peak fractions containing His_6-SUMO-FzlC were combined and His_6-Ulp1 (SUMO-protease) was added at 1:100 (protease:His_6-SUMO-FzlC) molar ratio. The His_6-SUMO tag was cleaved while dialyzing into FzlC Column Buffer A overnight at 4°C. Cleaved FzlC was incubated with Ni^{2+} Sepharose (GE Healthcare) for 1 h at 4°C after which the flow-through was collected. The Ni^{2+} Sepharose was then washed 3 times with 1 ml FzlC Column Buffer A. The flow-through and wash fractions containing FzlC were dialyzed overnight at 4°C in FzlC Storage Buffer (50 mM Tris-HCl pH 8.0, 300 mM KCl, 0.1 mM β-mercaptoethanol and 10% glycerol), concentrated if necessary, snap-frozen in liquid nitrogen and stored at −80°C.

To purify His_6-YFP-FzlC, Rosetta (DE3) pLysS *E. coli* cells were transformed with pEG420. The induction, harvesting and lysis were the same as for His_6-SUMO-FzlC. After centrifugation, the cleared supernatant was filtered and loaded on a HisTrap FF 1 ml column (GE Life Sciences) equilibrated in FzlC Column Buffer A. Protein was eluted with a linear gradient (1–100%) of FzlC Column Buffer B (same as Column Buffer A except 1 M imidazole). Peak fractions containing His_6-YFP-FzlC were combined and applied to a Superdex 200 10/300 GL column (GE Life Sciences) equilibrated in FzlC Storage Buffer. Peak fractions were combined, concentrated if necessary, snap-frozen in liquid nitrogen and stored at −80°C.

Cell fractionation

C. crescentus cells were fractionated as described previously (Jenal *et al.*, 1994) with slight modifications. 10 ml cultures of EG864 and EG1445 were grown in PYE to log phase and cells were centrifuged at 3,500*g* for 10 min. The pellets were resuspended in 1 ml Tris-HCl pH 7.5 and spun at maximum speed on a tabletop centrifuge for 2 min at 4°C. The pellets were resuspended in 1 ml lysis buffer (10 mM Tris-HCl pH 7.5, 1 mM EDTA, 250 μg ml^{-1} lysozyme) and incubated at room temperature for 10 min. Eight microliters of DNase was added and the cells were sonicated on ice. After centrifugation at 4,000*g* for 10 min at 4°C to remove intact cells, the supernatants were harvested and incubated on ice for 1 h. The lysates were centrifuged at 150,000*g* for 2h at 4°C. The supernatants were collected as the soluble "cytoplasmic fractions" and the pellets were subsequently washed twice with 10 mM Tris-HCl pH 7.5. The final pellets were resuspended in SDS-PAGE loading buffer with the same volumes as the soluble fractions and treated as the "membrane fractions."

Liposome preparation and sedimentation assay

Phosphatidylglycerol (PG) and/or L-α-phosphatidylcholine (Egg, Chicken PC) (Avanti Polar Lipids) in chloroform were transferred to glass tubes, dried under nitrogen gas and placed under vacuum for at least 1 h to remove residual chloroform. The lipids were resuspended in TK300 buffer (50 mM Tris-HCl pH 8.0, 300 mM KCl) and, if sucrose-loading the liposomes, sucrose was added to 170 mM final concentration. The glass tubes with resuspended lipids were covered in parafilm to prevent evaporation, incubated for at least 30 min at 42°C and sonicated and vortexed briefly every 10 min until the resuspended lipids appeared completely uniform. The multilamellar vesicles were then extruded with a 100 nm pore membrane. Sucrose-loaded vesicles were diluted at least 5× with non-sucrose containing TK300 buffer and centrifuged at 90,000*g* in a Beckman TLA-55 rotor in a table-top ultracentrifuge for 1 h at 25°C. The supernatant was discarded and the pellet containing the sucrose-loaded liposomes was resuspended in the appropriate volume of TK300. The resuspended liposomes were stored at 4°C for up to 2 weeks.

Sucrose-loaded liposomes (100 nm) of different percentages of PG and PC were prepared as described above in TK300 buffer. FzlC was quickly thawed and spun at 115,000*g* at 4°C for 15 min in a Beckman TLA-100 rotor and TL-100 ultracentrifuge to remove aggregates. FzlC (2 μM) was added to a suspension of 400 μM sucrose-loaded liposomes in TK300 buffer. Reactions were incubated at room temperature for 15 min. Sucrose-loaded vesicles were sedimented by centrifugation at 115,000*g* for 30 min at 25°C. About 90% of the supernatant was collected and 4× SDS-PAGE loading buffer was added to make a 1× mixture. The pellet was resuspended in 1× SDS-PAGE loading buffer to the same volume as the supernatant brought to 1×. The fraction of FzlC in the pellet was determined by running the samples on a SDS-PAGE gel, staining with Coomassie blue and performing densitometry on the bands.

Lipid preparation and GUV fabrication

Giant unilamellar vesicles were fabricated using the inverted emulsion technique (Pautot *et al.*, 2003; Luo *et al.*, 2014). For the inside monolayer 1-palmitoyl-2-oleoyl-*sn*-

glycero-3-phosphocholine (POPC) and 1-hexadecanoyl-2-(9Z-octadecenoyl)-*sn*-glycero-3-phospho-(1'-*rac*-glycerol) (POPG) at a 1:1 (wt:wt) ratio and for the outer layer L-α-phosphatidylcholine (Egg, Chicken PC) and 1-palmitoyl-2-oleoyl-*sn*-glycero-3-phospho-L-serine (POPS) at a 4:1 (wt:wt) ratio were aliquoted. All lipids were purchased from Avanti in their chloroform-solubilized form. Chloroform was evaporated overnight and the lipids were dissolved in hexadecane at 65°C for 3 h to obtain a 1 mg/ml stock solution. A 100 μl reaction containing YFP-FzlC, CFP-FtsZ, FtsZΔCTC-CFP or a combination of YFP-FzlC with either of the other two proteins were mixed with 10 mM phosphate-buffered saline (PBS) pH 7.6 and sucrose to obtain a 2 μM final concentration of each protein. $MgCl_2$ and GTP were added depending on the experimental condition. This solution was mixed with the inner leaflet-lipids and agitated for aqueous droplet formation. This phase was centrifuged (2500*g* for 6 min) over a stabilized monolayer of outer lipids that formed on top of a glucose solution. The GUVs were collected by punching a hole in the bottom of the centrifuge tube. Matching molar concentrations of glucose and sucrose were used to balance the osmotic pressure.

GUV imaging and image analysis

About 100 μl of GUVs were transferred to an 8-well plate and the GUVs were imaged with an inverted epi-fluorescence microscope (Axiovert135TV, ZEISS) using a 40× oil objective. QIClick charge-coupled camera (QImaging) was used to collect the fluorescence images. Exposure time was 10–50 ms depending on the channel and the intensity of the detected signal.

Image analysis was performed using MetaMorph®. Background fluorescent signal was subtracted from each GUV. A line scan was used to measure the fluorescent intensity across the diameter of each GUV. For YFP-FzlC and FtsZ-CFP +/– GTP conditions, this value was normalized based on the maximum signal intensity detected for each vesicle to enable comparison of signal between GUVs of different sizes. To determine the variation in protein, co-localization across different GUV populations' statistical analysis in *Prism*® was performed. The length and fluorescence intensity of each GUV was normalized. A cubic spline function was used to fit a fluorescent intensity curve for each vesicle. Standard deviation of this intensity was then calculated among a population of 18 GUVs.

FRET

FtsZ-CFP or FtsZΔCTC-CFP and/or YFP-FzlC (2 μM final concentration) were added to TK300 buffer. $MgCl_2$ was used at 2.5 mM, GTP was used at 2 mM and PG vesicles were used at 1 mg ml^{-1}. A Fluoromax-3 spectrofluorometer (Jobin Yvon) was used for fluorescence measurements. The solution was excited at 435 nm (CFP excitation) and scanned for emission from 450–560 nm. FRET/CFP ratios were determined by dividing peak YFP emission (523–528 nm) by peak CFP emission (472–477 nm).

FtsZ activity assays

FtsZ GTPase activity assay was performed in HEK50 buffer (50 mM HEPES-KOH, pH 7.2, 300 mM KCl and 0.1 mM EDTA). GTPase activity was assayed using the SensoLyte MG Phosphate Assay Kit (AnaSpec) following the manufacturer's protocol. The GraphPad Prism software was used to fit curves and determine GTPase rates.

Right angle light scattering was performed as described previously (Sundararajan *et al*., 2015).

TEM was performed as in (Sundararajan *et al*., 2015) with the following modifications: FtsZ and/or YFP-FzlC were used at 4 μM and the reaction buffer was TK300.

HADA labeling

Cells from strains EG444 and EG1062 were grown for 1 h in PYE with xylose to induce *ftsZ-yfp* expression, synchronized and the swarmers were released in fresh PYE. HADA (Kuru *et al*., 2012) was added to 0.41 mM after 30 min and cells were fixed and imaged as in (Sundararajan *et al*., 2015).

Acknowledgements

We thank Kousik Sundararajan for assistance with TEM; Yves Brun, Erkin Kuru and Michael van Nieuwenzhe for HADA; Lucy Shapiro, Brandon Williams, Patrick Viollier, Zemer Gitai, Martin Thanbichler and Thomas Bernhardt for plasmids, strains and/or antisera; Natalie Dye and Zach Pincus for assistance using CellTool; Christine Jacobs-Wagner for the demograph script; and Dan Georgess for guidance on statistical analysis. We would also like to thank Jie Xiao and the Xiao laboratory for helpful discussions and the Raben laboratory for invaluable assistance with lipid preparation. This work was funded by the JHUSOM, the Japan Science and Technology Agency (10216 to T.I.) and the National Institutes of Health under award numbers R01GM092930 (to T.I.) and R01GM108640 (to E.D.G.).

References

Beall, B., and Luktenhaus, J. (1992) Impaired cell division and sporulation of a *Bacillus subtilis* strain with the *ftsA* gene deleted. *J Bacteriol* **174**: 2389–2403.

Bowman, G.R. *et al*. (2010) *Caulobacter* PopZ forms a polar subdomain dictating sequential changes in pole composition and function. *Mol Microbiol* **76**: 173–189.

Buss, J., Coltharp, C., Huang, T., Pohlmeyer, C., Wang, S.C., Hatem, C., and Xiao, J. (2013) *In vivo* organization of the FtsZ-ring by ZapA and ZapB revealed by quantitative super-resolution microscopy. *Mol Microbiol* **89**: 1099–1120.

Cabre, E.J. *et al*. (2013) Bacterial division proteins FtsZ and ZipA induce vesicle shrinkage and cell membrane invagination. *J Biol Chem* **288**: 26625–26634.

Christen, B. *et al*. (2011) The essential genome of a bacterium. *Mol Syst Biol* **7**: 528–534.

Contreras, I., Shapiro, L., and Henry, S. (1978) Membrane phospholipid composition of *Caulobacter crescentus*. *J Bacteriol* **135**: 1130–1136.

Corbin, B.D., Wang, Y., Beuria, T.K., and Margolin, W. (2007) Interaction between cell division proteins FtsE and FtsZ. *J Bacteriol* **189**: 3026–3035.

Datta, P., Dasgupta, A., Bhakta, S., and Basu, J. (2002) Interaction between FtsZ and FtsW of *Mycobacterium tuberculosis*. *J Biol Chem* **277**: 24983–24987.

Din, N., Quardokus, E.M., Sackett, M.J., and Brun, Y.V. (1998) Dominant C-terminal deletions of FtsZ that affect its ability to localize in *Caulobacter* and its interaction with FtsA. *Mol Microbiol* **27**: 1051–1063.

Duman, R. *et al*. (2013) Structural and genetic analyses reveal the protein SepF as a new membrane anchor for the Z ring. *Proc Natl Acad Sci USA* **110**: E4601–E4610.

Erickson, H.P., Anderson, D.E., and Osawa, M. (2010) FtsZ in bacterial cytokinesis: cytoskeleton and force generator all in one. *Microbiol Mol Biol Rev* **74**: 504–528.

Geissler, B., Elraheb, D., and Margolin, W. (2003) A gain-of-function mutation in *ftsA* bypasses the requirement for the essential cell division gene *zipA* in *Escherichia coli*. *Proc Natl Acad Sci USA* **100**: 4197–4202.

Goley, E.D., Comolli, L.R., Fero, K.E., Downing, K.H., and Shapiro, L. (2010a) DipM links peptidoglycan remodelling to outer membrane organization in *Caulobacter*. *Mol Microbiol* **77**: 56–73.

Goley, E.D., Dye, N.A., Werner, J.N., Gitai, Z., and Shapiro, L. (2010b) Imaging-based identification of a critical regulator of FtsZ protofilament curvature in *Caulobacter*. *Mol Cell* **39**: 975–987.

Goley, E.D., Yeh, Y.C., Hong, S.H., Fero, M.J., Abeliuk, E., McAdams, H.H., and Shapiro, L. (2011) Assembly of the *Caulobacter* cell division machine. *Mol Microbiol* **80**: 1680–1698.

Guo, L.W., Assadi-Porter, F.M., Grant, J.E., Wu, H., Markley, J.L., and Ruoho, A.E. (2007) One-step purification of bacterially expressed recombinant transducing α-subunit and isotopically labeled PDE6 γ-subunit for NMR analysis. *Protein Expr Purif* **51**: 187–197.

Gupta, S., Banerjee, S.K., Chatterjee, A., Sharma, A.K., Kundu, M., and Basu, J. (2015) The essential protein SepF of *Mycobacteria* interacts with FtsZ and MurG to regulate cell growth and division. *Microbiology* **161**: 1627–1638.

Hale, C.A., and de Boer, P.A. (1997) Direct binding of FtsZ to ZipA, an essential component of the septal ring structure that mediates division in *E. coli*. *Cell* **88**: 175–185.

Jenal, U., White, J., and Shapiro, L. (1994) *Caulobacter* flagellar function, but not assembly, requires FliL, a non-polarly localized membrane protein present in all cell types. *J Mol Biol* **243**: 227–244.

Jensen, S.O., Thompson, L.S., and Harry, E.J. (2005) Cell division in *Bacillus subtilis*: FtsZ and FtsA association is Z-ring independent, and FtsA is required for efficient mid-cell Z-ring assembly. *J Bacteriol* **187**: 6536–6544.

Judd, E.M., Comolli, L.R., Chen, J.C., Downing, K.H., Moerner, W.E., and McAdams, H.H. (2005) Distinct constrictive processes, separated in time and space, divide *Caulobacter* inner and outer membranes. *J Bacteriol* **187**: 6874–6882.

Kuru, E. *et al*. (2012) *In situ* probing of a newly synthesized peptidoglycan in live bacteria with fluorescent D-amino acids. *Angew Chem Int Ed* **51**: 12519–12523.

Lee, T.K., and Huang, K.C. (2013) The role of hydrolases in bacterial cell-wall growth. *Curr Opin Microbiol* **16**: 760–766.

Loose, M., and Mitchison, T.J. (2014) The bacterial cell division proteins FtsA and FtsZ self-organize into dynamic cytoskeletal patterns. *Nat Cell Biol* **16**: 38–46.

Luo, T., Srivastava, V., Ren, Y., and Robinson, D.N. (2014) Mimicking the mechanical properties of the cell cortex by the self-assembly of an actin cortex in vesicles. *Appl Phys Lett* **104**: 153701–153705.

Martin, M.E., Trimble, M.J., and Brun, Y.V. (2004) Cell cycle-dependent abundance, stability and localization of FtsA and FtsQ in *Caulobacter crescentus*. *Mol Microbiol* **54**: 60–74.

Mavrici, D. *et al*. (2014) *Mycobacterium tuberculosis* FtsX extracellular domain activates the peptidoglycan hydrolase, RipC. *Proc Natl Acad Sci USA* **111**: 8037–8042.

Meier, E.L., and Goley, E.D. (2014) Form and function of the bacterial cytokinetic ring. *Curr Opin Cell Biol* **26**: 19–27.

Meisner, J., Montero-Llopis, P., Sham, L.T., Garner, E., Bernhardt, T.G., and Rudner, D.Z. (2013) FtsEX is required for CwlO peptidoglycan hydrolase activity during cell wall elongation in *Bacillus subtilis*. *Mol Microbiol* **89**: 1069–1083.

Möll, A., Schlimpert, S., Briegel, A., Jensen, G.J., and Thanbichler, M. (2010) DipM, a new factor required for peptidoglycan remodeling during cell division in *Caulobacter crescentus*. *Mol Microbiol* **77**: 90–107.

Möll, A., and Thanbichler, M. (2009) FtsN-like proteins are conserved components of the cell division machinery in proteobacteria. *Mol Microbiol* **72**: 1037–1053.

Ohta, N., Ninfa, A.J., Allaire, A., Kulick, L., and Newton, A. (1997) Identification, characterization, and chromosomal organization of cell division cycle genes in *Caulobacter crescentus*. *J Bacteriol* **179**: 2169–2180.

Osawa, M., Anderson, D.E., and Erickson, H.P. (2008) Reconstitution of contractile FtsZ rings in liposomes. *Science* **320**: 792–794.

Osawa, M., and Erickson, H.P. (2013) Liposome division by a simple bacterial division machinery. *Proc Natl Acad Sci USA* **110**: 11000–11004.

Osley, M.A., and Newton, A. (1977) Mutational analysis and developmental control in *Caulobacter crescentus*. *Proc Natl Acad Sci USA* **74**: 124–128.

Pautot, S., Frisken, B.J., and Weitz, D.A. (2003) Engineering asymmetric vesicles. *Proc Natl Acad Sci USA* **100**: 10718–10721.

Pichoff, S., and Lutkenhaus, J. (2002) Unique and overlapping roles for ZipA and FtsA in septal ring assembly in *Escherichia coli*. *EMBO J* **21**:685–693.

Pichoff, S., Shen, B., Sullivan, B., and Luktenhaus, J. (2012) FtsA mutants impaired for self-interaction bypass ZipA suggesting a model in which FtsA's self-interaction competes with its ability to recruit downstream division proteins. *Mol Microbiol* **83**: 151–167.

Pichoff, S., Du, S., and Lutkenhaus, J. (2015) The bypass of ZipA by overexpression of FtsN requires a previously unknown conserved FtsN motif essential for FtsA-FtsN interaction supporting a model in which FtsA monomers

recruit late cell division proteins to the Z ring. *Mol Microbiol* **95**: 971–987.
Pincus, Z., and Theriot, J.A. (2007) Comparison of quantitative methods for cell-shape analysis. *J Microscopy* **227**: 140–156.
Potluri, L.P., Kannan, S., and Young, K.D. (2012) ZipA is required for FtsZ-dependent preseptal peptidoglycan synthesis prior to invagination during cell division. *J Bacteriol* **194**: 5334–5342.
Radhakrishnan, S.K., Thanbichler, M., and Viollier, P.H. (2008) The dynamic interplay between a cell fate determinant and a lysozyme homolog drives the asymmetric division cycle of *Caulobacter crescentus*. *Genes Dev* **22**: 212–225.
Sham, L.T., Barendt, S.M., Kopecky, K.E., and Winkler, M.E. (2011) Essential PcsB putative peptidoglycan hydrolase interacts with the essential FtsXSpn cell division protein in *Streptococcus pneumonia* D39. *Proc Natl Acad Sci USA* **108**: E1061–E1069.
Singh, J.K., Makde, R.D., Kumar, V., and Panda, D. (2007) A membrane protein, EzrA, regulates assembly dynamics of FtsZ by interacting with the C-terminal tail of FtsZ. *Biochemistry* **46**: 11013–11022.
Sliusarenko, O., Heinritz, J., Emonet, T., and Jacobs-Wagner, C. (2011) High-throughput, subpixel precision analysis of bacterial morphogenesis and intracellular spatio-temporal dynamics. *Mol Microbiol* **80**: 612–627.
Sundararajan, K., Miguel, A., Desmarais, S.M., Meier, E.L., Huang, K.C., and Goley, E.D. (2015) The bacterial tubulin FtZ requires its intrinsically disordered linker to direct robust cell wall construction. *Nat Commun* **6**: 7281.
Uehara, T., Parzych, K.R., Dinh, T., and Bernhardt, T.G. (2010) Daughter cell separation is controlled by cytokinetic ring-activated cell wall hydrolysis. *EMBO J* **29**: 1412–1422.
Vaughan, S., Wickstead, B., Gull, K., and Addinall, S.G. (2004) Molecular evolution of FtsZ protein sequences encoded within the genomes of archaea, bacteria, and eukaryote. *J Mol Evol* **58**: 19–29.
Yakhnina, A.A., and Gitai, Z. (2013) Diverse functions for six glycosyltransferases in *Caulobacter crescentus* cell wall assembly. *J Bacteriol* **195**: 4527–4535.
Yang, D.C., Peters, N.T., Parzych, K.R., Uehara, T., Markovski, M., and Bernhardt, T.G. (2011) An ATP-binding cassette transporter-like complex governs cell-wall hydrolysis at the bacterial cytokinetic ring. *Proc Natl Acad Sci USA* **108**: E1052–E1060.

Supporting information

Additional supporting information may be found in the online version of this article at the publisher's web-site.